High-Performance Ferroelectric Polymer Side-Gated CdS Nanowire Ultraviolet Photodetectors

Dingshan Zheng, Hehai Fang, Peng Wang, Wenjin Luo, Fan Gong, Johnny C. Ho, Xiaoshuang Chen, Wei Lu, Lei Liao, Jianlu Wang,* and Weida Hu**

An efficient ferroelectric-enhanced side-gated single CdS nanowire (NW) ultraviolet (UV) photodetector at room temperature is demonstrated. With the ultrahigh electrostatic field from polarization of ferroelectric polymer, the depletion of the intrinsic carriers in the CdS NW channel is achieved, which significantly reduces the dark current and increases the sensitivity of the UV photodetector even after the gate voltage is removed. Meanwhile, the low frequency noise current power of the device reaches as low as 4.6×10^{-28} A^2 at a source-drain voltage V_{ds} = 1 V. The single CdS NW UV photodetector exhibits high photoconductive gain of 8.6×10^5, responsivity of 2.6×10^5 A W^{-1}, and specific detectivity (D^*) of 2.3×10^{16} Jones at a low power density of 0.01 mW cm^{-2} for λ = 375 nm. In addition, the spatially resolved scanning photocurrent mapping across the device shows strong photocurrent signals near the metal contacts. This is promising for the design of a controllable, high-performance, and low power consumption ultraviolet photodetector.

1. Introduction

In the past few decades, UV photodetectors have been widely used in air and water sterilization, environmental monitoring, optical imaging, flame sensing and fire detection, military, and space, etc.[1–3] UV photodetectors based on 1D semiconductor nanostructures, for example, ZnO,[3] SnO_2,[4] ZnS,[5] and GaN,[6] have already been fabricated. However, a large dark current and a low I_{light}/I_{dark} ratio are found in these devices, which are mainly caused by the concentration of defect/trap induced carriers, resulting in lower specific detectivity (D^*).[2] Although operating the device at the OFF state by applying a large negative gate voltage brings out the advantage of a reduced dark current, it would cause a large power consumption.[7,8] Therefore, in order to suppress the dark current of the device, it is necessary to deplete those defect/trap induced carriers through special methods, such as designing a unique device structure. Recently, Poly(vinylidene fluoride-trifluoroethylene) [P(VDF-TrFE)] ferroelectric polymer film has been employed in various nanoelectronic and optoelectronic devices due to its room temperature ultrahigh ferroelectricity, large remnant polarization, and stable retention characteristics.[8–13] An ultrahigh local electrostatic field induced by the stable remnant polarization of the P(VDF-TrFE) ferroelectric polymer film is larger than that produced by the gate voltage in traditional NW field-effect transistors (FETs).[8,10] Thus, the depletion of the intrinsic carriers can be achieved by the stable remnant polarization of the P(VDF-TrFE) ferroelectric polymer even when the negative gate voltage is removed.

As a typical II–VI semiconductor with direct band gap (2.4 eV), cadmium sulfide (CdS) nanowires (NWs), nanorods (NRs), and nanobelts (NBs) have demonstrated great potential in electronic and optoelectronic applications, such as lasers,[14] light-emitting diodes,[15] optical switches,[16] solar cells,[17,18] photodetectors,[19–28] gas sensors,[20,29] and logic circuit.[30] Among these applications, UV–visible photodetectors based on CdS nanostructure materials have been widely investigated and exhibited potential applications due to their large surface-to-volume ratio, rich surface state, remarkable optoelectronic characteristics, and UV–visible light absorption.[20,21,28] It has been reported that Schottky-gated CdS NW UV–visible photodetectors show much higher detection sensitivity and much shorter reset time than that of the ohmic contact based devices,[24] and visible photodetectors based on CdS NB exhibit ultrahigh responsivity of 7.3×10^4 A W^{-1} and quantum efficiency of 1.9×10^7%, but there is a large dark current that limits its detectivity.[27]

In this work, we fabricated ferroelectric polymer side-gated single CdS NW UV photodetector by a relatively simple manufacturing process. The intrinsic carriers in the NW channel can be fully depleted by the ultrahigh electrostatic field from polarization of P(VDF-TrFE) ferroelectric polymer with a pulsed

Dr. D. Zheng, Dr. F. Gong, Prof. L. Liao
Department of Physics and Key Laboratory of Artificial Micro- and Nano-structures of Ministry of Education
Wuhan University
Wuhan 430072, China
E-mail: liaolei@whu.edu.cn

Dr. D. Zheng, Dr. H. Fang, Dr. P. Wang, Dr. W. Luo, Dr. F. Gong, Prof. X. Chen, Prof. W. Lu, Prof. J. Wang, Prof. W. Hu
National Laboratory for Infrared Physics
Shanghai Institute of Technical Physics
Chinese Academy of Sciences
Shanghai 200083, China
E-mail: jlwang@mail.sitp.ac.cn; wdhu@mail.sitp.ac.cn

Prof. J. C. Ho
Department of Physics and Materials Science
City University of Hong Kong
Hong Kong SAR, China

DOI: 10.1002/adfm.201603152

© 2016 WILEY-VCH Verlag GmbH & Co. KGaA, Weinheim

gate bias of −20 V, which significantly reduces the dark current and increases the detectivity of the photodetector. Even if the gate voltage pulse is removed, the device can still keep the full-depleted state induced by unchanged polarization, indicating that our devices can work without additional negative gate bias. Noise characteristics and noise equivalent power (NEP) of the depleted CdS NW photodetectors are also measured and analyzed. Utilizing this device structure, the CdS NW UV photodetector exhibits high photoconductive gain of 8.6×10^5, responsivity of 2.6×10^5 A W^{-1}, and specific detectivity (D^*) up to 2.3×10^{16} Jones at a low power density of 0.01 mW cm^{-2} for $\lambda = 375$ nm.

2. Results and Discussion

The single-crystalline CdS NWs with the lengths of tens of micrometers and diameters of 50–300 nm were synthesized by a chemical vapor deposition (CVD) method that was reported in our previous work.[12] The photoluminescence spectrum of CdS NWs shows a strong and sharp peak around 505 nm (Figure S1, Supporting Information), which is consistent with the previous reports.[14,19,20] The schematic diagrams and scanning electron microscope (SEM) image of our ferroelectric side-gated single CdS NW photodetector are shown in **Figure 1**a–c, respectively. A typical ferroelectric hysteresis loop of P(VDF-TrFE) capacitor was measured (Figure S2, Supporting Information). The coercive voltage is about 11.5 V and the remnant polarization value P_r is about 6.2 μC cm^{-2}, indicating that the ferroelectric polymer has remarkable polarization properties.[8] To further investigate the photocurrent response of the CdS NW photodetector, the photocurrent mapping was performed by a scanning photocurrent microscopy. Figure 1d shows the spatially resolved mapping of the photocurrent across the device under a 450 nm laser excitation (90 μW), at source-drain voltage $V_{ds} = 0.1$ V. The image clearly displays that strong photocurrent signals are generated at the metal contacts, which are attributed to the efficient separation of photon-generated electron–hole pairs in CdS NW by local built-in electric fields.[31–35] The relatively weak photocurrent signals along the NW are due to the recombination of photon-generated electron–hole pairs before being collected by the source/drain electrodes.[32,35]

The I_{ds}–V_{gs} transfer characteristics of the CdS NW FET with P(VDF-TrFE) ferroelectric polymer film were investigated at $V_{ds} = 1$ V, as shown in **Figure 2**a. The device shows a high I_{on}/I_{off} ratio of $>10^6$. The low off current of $<10^{-12}$ A is obtained when a negative gate voltage V_{gs} of less than −13 V is applied. When a negative V_{gs} of −20 V with the pulse width of 2 s is employed to gate electrode, the polarization of the ferroelectric polymer film will be aligned to the gate electrode under the negative electrostatic field gradient. This ultrahigh electrostatic field induced by polarization of P(VDF-TrFE) ferroelectric polymer results in depletion of free electrons in the n-typed CdS NW channel, as depicted in Figure 1b. In this scenario, the dark current is suppressed and reduced to less than 10^{-12} A due to the remnant polarization of the P(VDF-TrFE) ferroelectric polymer, even after the gate voltage is removed. In addition, the retention properties of the device after depletion were measured (Figure S2b, Supporting Information). The device demonstrates stable retention characteristics (over 50 000 s) at room temperature. The long-time stability indicates that our devices can work as a two-terminal device. The ferroelectric hysteresis window of ≈9 V is caused by the remnant polarization of the ferroelectric polymer film. Notably, the ferroelectric remains polarized and the on-state remains stable, when V_{gs} sweeps range is taken from +20 to −20 V. The polarizations of the ferroelectric dielectric start to change sign with the negative V_{gs} increases and I_{ds} changes from on-state to off-state. The side-gated NW device with ferroelectric polymer film exhibits a counterclockwise hysteresis loop, which is opposite to the clockwise hysteresis of back-gated NW device (Figure S3, Supporting Information), demonstrating that the transfer characteristics of the device are strongly influenced by the polarization of P(VDF-TrFE) ferroelectric polymer.[13]

The photoresponse behaviors of CdS NW UV photodetector were investigated at room temperature. Figure 2b presents the

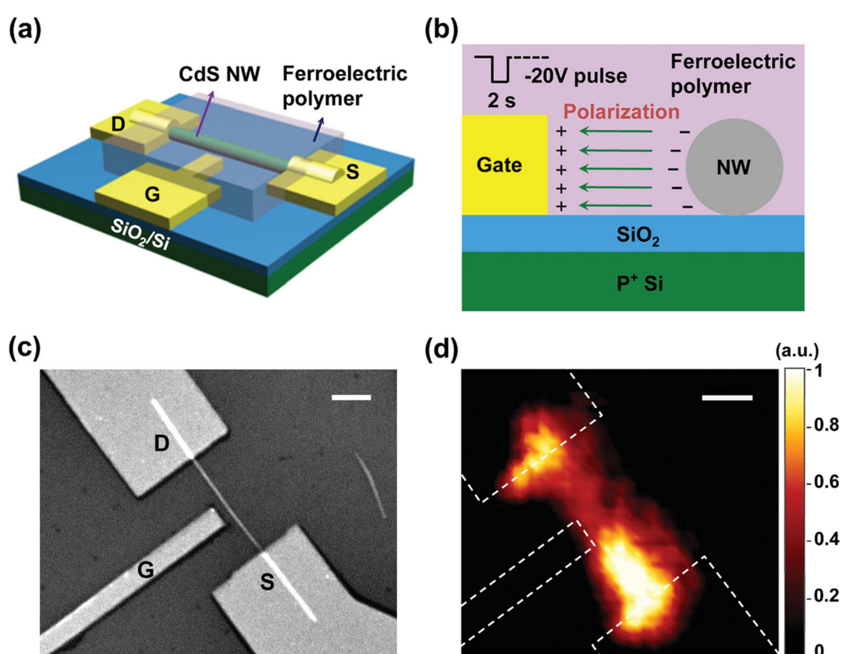

Figure 1. Structure, schematic diagram, and photocurrent image of ferroelectric side-gated single CdS NW photodetector. a) A schematic illustration of ferroelectric side-gated single CdS NW photodetector. b) The cross-sectional structure and schematic diagram of the device operating in negative polarization state (depleted state). Electrons in the NW channel will be depleted by a pulse V_{gs} of −20 V and the pulse width of 2 s. c) SEM image of CdS NW FET, the channel length (L) is 3.1 μm, the NW diameter (d) is 110 nm, and the distance between NW and gate electrode is 260 nm, respectively. The scale bar is 1 μm. d) Spatially resolved photocurrent mapping of the device under a 450 nm laser excitation (90 μW), at $V_{ds} = 0.1$ V. The outlines of the electrodes are shown as dotted lines. The scale bar is 1 μm.

© 2016 WILEY-VCH Verlag GmbH & Co. KGaA, Weinheim

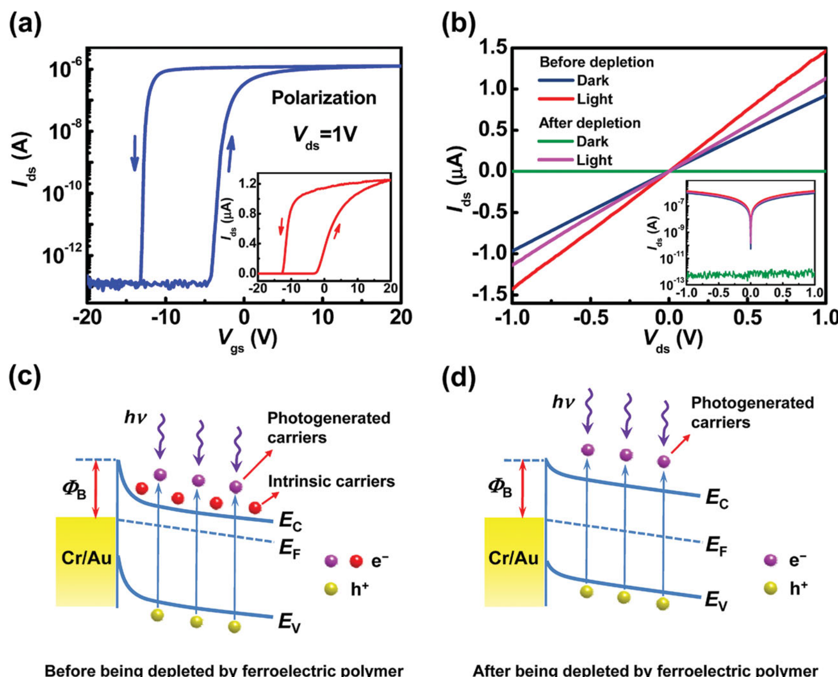

Figure 2. Ferroelectric-enhanced photoresponse and energy band diagrams of the ferroelectric side-gated single CdS NW UV photodetector. a) The I_{ds}–V_{gs} transfer curves of CdS NW FET with P(VDF-TrFE) ferroelectric polymer. The inset is the linear curve. b) I_{ds}–V_{ds} characteristics of the UV photodetector in the dark and under UV illumination (375 nm, 18 mW cm^{-2}), before and after being depleted by ferroelectric polymer film. c,d) The corresponding energy band diagrams of two different states under UV illumination at a drain–source bias, before and after being depleted by ferroelectric polymer film. E_F is the Fermi level energy, E_C is the minimum conduction band energy, E_V is the maximum valence band energy, and Φ_B is the Schottky barrier height. E_C and E_V bend upward in the full-depleted state, respectively.

I_{ds}–V_{ds} characteristics of the device in the dark and under UV illumination (375 nm, 18 mW cm^{-2}), before and after being depleted by ferroelectric polymer film, without additional gate voltage. I_{dark} is the original current before the device was illuminated, and I_{light} is the current under UV illumination. The net photocurrent is defined as $I_{ph} = |I_{light}| - |I_{dark}|$. Before being depleted, I_{ph} = 0.55 μA is obtained at V_{ds} = 1 V. The device shows a low I_{ph}/I_{dark} ratio (<1), which can be attributed to a large dark current. While after being depleted, I_{dark} is reduced to ≈10^{-12} A, and the net photocurrent I_{ph} = 1.13 μA, leading to a much high ratio of I_{ph}/I_{dark} ≈10^6 is obtained at V_{ds} = 1 V. The photoresponse behaviors of UV photodetector can be explained by the schematic energy band diagrams, as shown in Figure 2c,d. Before being depleted, thermionic/tunneling currents induced by the intrinsic carriers and photon-generated current induced by the excited electron–hole pairs contribute to the channel current,[7,36] I_{light} = 1.46 μA. After being depleted, thermionic/tunneling currents have no contribution to the channel current, and the photon-generated current dominants the channel current, thus I_{light} decreases slightly, I_{light} = 1.13 μA. However, I_{dark} is reduced significantly after being depleted, resulting in a high ratio of I_{ph}/I_{dark}.

For the following investigations, the depletion of the intrinsic carriers was pre-achieved by a short V_{gs} pulse of −20 V and the pulse width of 2 s on the side gate. **Figure 3**a presents the I_{ds}–V_{ds} characteristics of ferroelectric polymer film side-gated single CdS NW UV photodetector for different UV intensities at a wavelength of 375 nm after being depleted, without additional gate voltage. The photocurrent under different UV intensities was extracted and plotted in Figure 3b, at V_{ds} = 1 V. The relationship between the photocurrent and UV intensity can be expressed as[37,38]

$$I_{ph} = cP^k \quad (1)$$

where I_{ph} is the photocurrent, c is a proportionality constant, P is the incident power density, and k is an empirical value. Through the power function nonlinear fitting, we can obtain k = 0.6, depending on the complex processes of electron–hole generation, trapping, and recombination.[38]

The photoconductive gain (G), responsivity (R), and specific detectivity (D^*) are the key parameters to evaluate the sensitivity of the photodetectors.[1] The photoconductive gain is defined as the ratio between the number of charges collected by the electrodes per unit time and the number of photons absorbed by the NW per unit time ($G = N_e/N_{ph}$), which can be expressed as[2,3,39]

$$G = (I_{ph}/e)/(PA/h\nu) \quad (2)$$

where P is the incident power density, $h\nu$ is the energy of an incident photon, e is the electronic charge, and A is the effective irradiated area on the NW. To estimate the response of

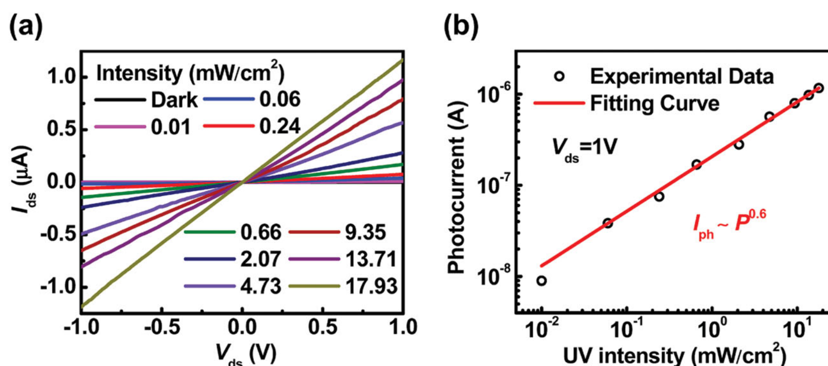

Figure 3. Photoresponse properties of the ferroelectric side-gated single CdS NW UV photodetector. a) I_{ds}–V_{ds} characteristics of the UV photodetector in the dark and under different UV intensities (375 nm) after being depleted, without additional gate voltage. b) Dependence of photocurrent on different UV intensities, at V_{ds} = 1 V.

© 2016 WILEY-VCH Verlag GmbH & Co. KGaA, Weinheim

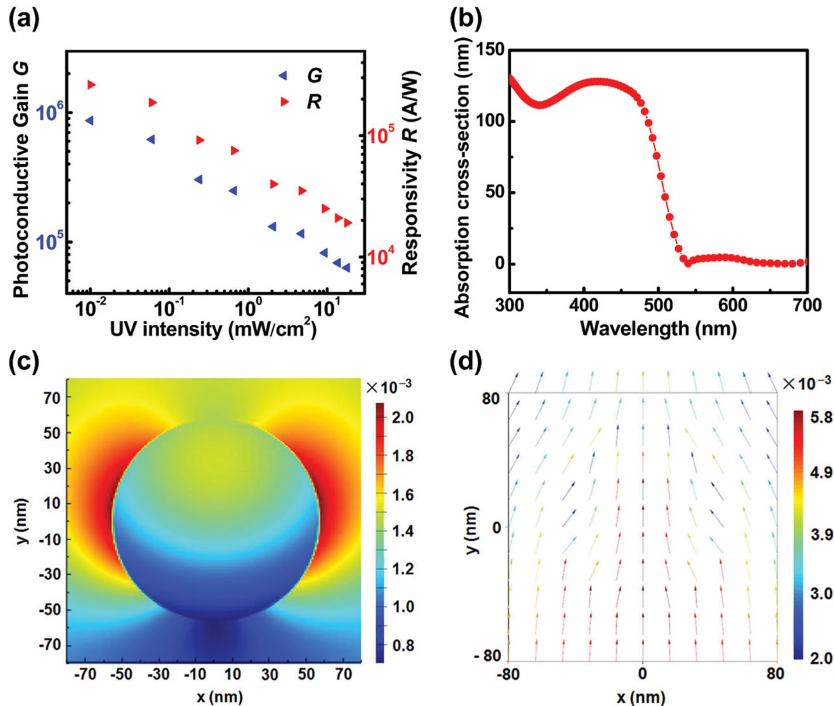

Figure 4. Photoconductive gain and responsivity of the UV photodetector, and the simulation of the absorption cross section of the NW. a) Dependence of photoconductive gain and responsivity on different UV intensities, at $V_{ds} = 1$ V. b) Dependence of the absorption cross section δ of the CdS NW on illumination wavelengths. c) The optical energy and d) the Poynting vector distribution when the incident light is perpendicular to the surface of the NW. The simulation was carried out using the finite-difference time-domain (FDTD) method.

the photocurrent to the incident power, the responsivity of a photodetector can be calculated according to the following expression[2,40,41]

$$R = I_{ph}/(PA) \tag{3}$$

where I_{ph} is the photocurrent. **Figure 4**a presents the calculated values of G and R at different UV intensities. The long photon-generated electrons' lifetime in the NW compared to the short electrons' transport time between the electrodes results in a high photoconductive gain.[3] Figure 4a shows that G and R increase dramatically with the decreasing UV intensity, and the G and R are up to 8.6×10^5 and 2.6×10^5 A W^{-1} at $V_{ds} = 1$ V and under the low UV intensity of 0.01 mW cm^{-2}. Here, the cross-sectional area of the NW, $A = L \times d$, is considered as an estimation of the effective irradiated area.[3,12] The light absorption of the NW was simulated using the finite-difference time-domain (FDTD) methods. Based on the assumption that the NW is ideal and has an infinite length, the total absorption cross section for different illumination wavelengths was simulated and plotted in Figure 4b. Due to the reflection and scattering of light and antenna-like structure of the NW, the absorbed light energy is not equal to the light energy irradiated on the cross section of the NW. Figure 4c,d presents the optical energy and Poynting vector distribution when the incident light is perpendicular to the surface of the NW. Figure 4c shows that the optical energy varies gradually over the cross section of the NW due to the absorption and scattering of light. The absorption power of simulated NW can be expressed as $P_i = P \times L \times \delta$, where P is the incident power density, L is the channel length, and δ is the absorption cross section. There are two absorption peaks at least in Figure 4b. The absorption peak at the wavelength shorter than 350 nm and the absorption peak at 420 nm may be mainly attributed to the intrinsic absorption as well as the resonance of the incident light and antenna-like structure of the NW. The absorption cross section $\delta = 120$ nm is obtained at 375 nm, which is close to the NW diameter $d = 110$ nm in the experiment. Although the intrinsic absorption varies with the incident wavelength, they have the same order of magnitude. Thus, it is reasonable to consider the cross-sectional area of the NW ($A = L \times d$) as the effective irradiated area of the NW.

NEP and the specific detectivity (D^*) are also important parameters for a photodetector, which are limited mainly by three major noise sources, namely, flicker noise ($1/f$ noise), Johnson noise, and shot noise from the dark current.[40,42] Noise power density spectra of the CdS NW photodetectors were measured after being depleted using a noise spectrum analyzer. **Figure 5**a shows that the low-frequency noise characteristics of the device measured at 1 V bias and under the dark condition is close to the background signals measured at 0 V bias. The noise power density $S_n(f)$ can be fitted using Equation (4)[43,44]

$$S_n(f) = K \frac{I_d^{\beta}}{f^{\alpha}} \tag{4}$$

where K is a constant, I_d is the dark current, f is the frequency, and α and β are two fitting parameters. The fitting result shows that $\alpha = 1.06$ is nearly uniform over the measured frequency range, which indicates a typical $1/f$ noise behavior.[19,43] Note that no Johnson and shot noise are evidently observed at low-frequency range, which are mainly attributed to the lower dark current of the device.[44,45] These two noises are independent of the frequency, and they are white noise types. Therefore, the low-frequency noise of the device is dominated by the $1/f$ noise. In addition, low-frequency noise power spectra of CdS NW photodetector under different applied bias voltages were measured (Figure S4, Supporting Information), which shows that the low-frequency noise characteristics of the device measured at 0.1 V bias are also close to the background signals measured at 0 V bias. The total noise current power of the device can be estimated by integrating $S_n(f)$ over the measured frequency range[43,45]

$$\langle i_n \rangle^2 = \int_0^B S_n(f)\,df = \int_0^1 S_0\,df + \int_1^B \frac{S_0}{f}\,df = S_0\left[\ln(B) + 1\right] \tag{5}$$

© 2016 WILEY-VCH Verlag GmbH & Co. KGaA, Weinheim

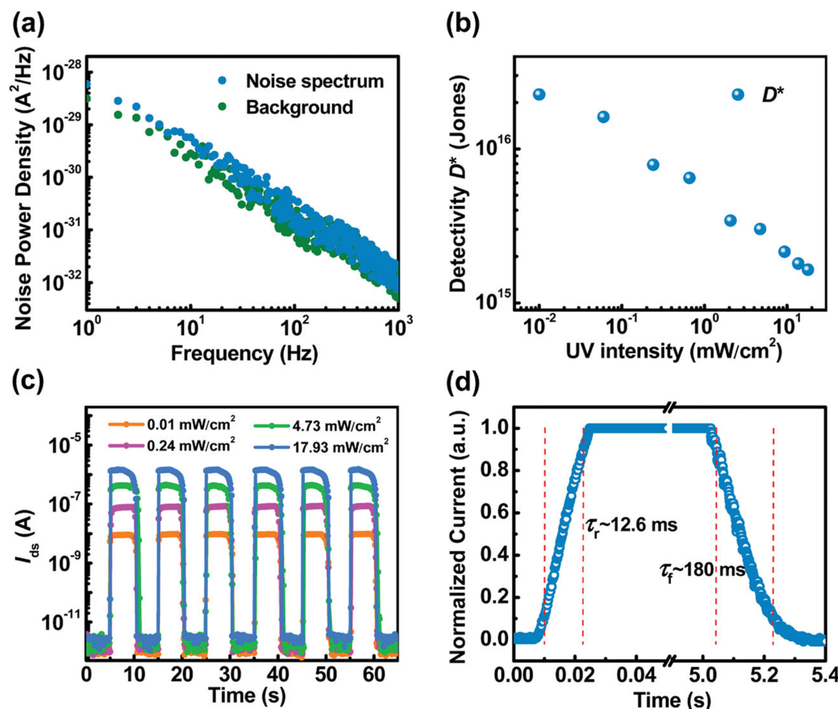

Figure 5. Noise, detectivity, and time-response characterizations of the ferroelectric side-gated single CdS NW UV photodetector. a) Noise power spectrum of the device at V_{ds} = 1 V. The background noise was also measured for comparison. b) The specific detectivity of the photodetector under different UV intensities, at V_{ds} = 1 V. c) Photocurrent response of the device under UV illumination with different intensities, the UV light is turned on/off at an interval of 5 s, at V_{ds} = 1 V, after being depleted and without additional gate voltage. d) Time-resolved photoresponse of the device, the rise and fall of the photocurrent, and the fitted data using exponential functions, at V_{ds} = 1 V.

where $S_n(f)$ in the bandwidth range from 0 to 1 is assumed to be constant and equal to $S_0[S_n(f = 1\text{ Hz})]$. B = 1 kHz is the bandwidth. The total noise current power, i.e., the flicker noise current power $\langle i_n \rangle^2$ is obtained to be ≈4.6 × 10^{-28} A^2. The flicker noise current is ≈2.1 × 10^{-14} A. Thus, the NEP and D^* can be calculated according to Equations (6) and (7)[42–45]

$$\text{NEP} = \frac{\sqrt{\langle i_n \rangle^2}}{R} \quad (6)$$

$$D^* = \frac{\sqrt{A}\sqrt{B}}{\text{NEP}} \quad (7)$$

where R is the responsivity, A is the effective area of the detector, B is the bandwidth. Figure 5b presents the calculated values of D^* at different UV intensities. It shows that the D^* is up to 2.3 × 10^{16} Jones at V_{ds} = 1 V, under the low UV intensity of 0.01 mW cm^{-2}. For a wider frequency range, the shot noise from dark current at large bandwidth will be the major contribution limiting the detectivity.[2,40] Overall, with the ultrahigh ferroelectric polarization field of P(VDF-TrFE) ferroelectric polymer, we achieve the full depletion of the intrinsic carriers in the NW channel, which significantly reduces the dark current and increases the sensitivity of the photodetector. High photoconductive gain and responsivity, low dark current, and noise current, lead to detectivity of UV photodetector as high as 2.3 × 10^{16} Jones. The devices show better performances compared with those reported detectors based on CdS nanostructure.[21,26,27]

To further investigate the response speed of the photodetector, time-resolved photoresponse measurements were performed by periodically turning on and off the UV light (375 nm). The photocurrent responses under UV illumination with different intensities are shown in Figure 5c, after being depleted and without additional gate voltage. A high speed oscilloscope was used to monitor the fast-varying optical signal.[38] The response time (rise time τ_r), defined as the time for the photocurrent increasing from 10% to 90% I_{peak}, is 12.6 ms, and the recovery time (fall time τ_f), defined as the time decreasing from 90% to 10% I_{peak}, is 180 ms, respectively, as shown in Figure 5d. The longer recovery time may be related to the influence of the surface states and the crystal quality of CdS NWs.[7,38] Furthermore, the recombination of photogenerated electrons and holes may be affected by the surface defect states of CdS NW and the interface states between the CdS NW and P(VDF-TrFE) ferroelectric polymer.[8] The time-resolved photoresponse measurement of the device was performed before being depleted (Figure S5a, Supporting Information), which shows a low ratio of I_{light}/I_{dark}. In addition, the photoresponse of the device was achieved under deep UV illumination at a wavelength of 280 nm (≈5 mW cm^{-2}), after being depleted and without additional gate voltage (Figure S5b, Supporting Information), indicating that the ferroelectric-enhanced side-gated CdS NW photodetector is also sensitive to the deep UV light.

3. Conclusion

In summary, we have fabricated the ferroelectric polymer side-gated CdS NW UV photodetectors. The dark current of the device is reduced significantly after being depleted by the ultrahigh electrostatic field from polarization of ferroelectric polymer with a short negative gate voltage pulse on the side gate. The flicker noise (1/f noise) is the dominant noise source of the detectors, and the flicker noise power is as low as ≈4.6 × 10^{-28} A^2 at V_{ds} = 1 V. The ferroelectric polymer side-gated single CdS NW UV photodetector exhibits an ultrahigh detection performance with high photoconductive gain of 8.6 × 10^5, responsivity of 2.6 × 10^5 A W^{-1}, and specific detectivity of 2.3 × 10^{16} Jones at a low power density of 0.01 mW cm^{-2} for λ = 375 nm, which are higher than traditional FET UV photodetectors. These results demonstrate that a new approach is established to fabricate controllable, high-performance, and low power consumption UV photodetector.

© 2016 WILEY-VCH Verlag GmbH & Co. KGaA, Weinheim

4. Experimental Section

Nanowires Synthesis: The single-crystalline CdS NWs were synthesized via a CVD method. CdS powder was placed onto a ceramic boat at the center of a quartz tube, and silicon substrate coated with 1 nm thick of Au catalyst was placed at the downstream of the carrier gas flow. After the tube was pumped down to a pressure of 1×10^{-3} mbar, a mixture gas (argon/hydrogen = 100:20) was introduced into the quartz tube at a flow rate of 50 sccm (standard-state cubic centimeter per minute). The CdS powder is heated to 700 °C and maintained for about 50 min at a pressure of 100 mbar. After the system was cooled down to room temperature, a large amount of CdS NWs was found on the surface of the silicon substrate.

UV Photodetectors Fabrication and Characterization: The CdS NWs were transferred onto the Si/SiO_2 (110 nm) substrate. Then the substrate was spin-coated with MMA and PMMA, and electron-beam lithography (JEOL 6510 with NPGS system) technique was employed to define the drain, source, and side-gate patterns. The Cr/Au (15 nm/50 nm) electrodes were fabricated by metal evaporation and lift-off processes. A 200 nm of P(VDF-TrFE) (70:30 in mol%) ferroelectric polymer film was deposited on the NW channel by spin coating, followed by an annealing step to improve its crystallinity at 130 °C for 2 h on a hot plate. The optoelectronic measurements of fabricated NW photodetectors were performed with the Lake Shore TTPX Probe Station and Keithley 4200 semiconductor characterization system. The photocurrent map was acquired by scanning the sample under a focused laser beam through a 100X Nikon lens. Noise power spectra of the photodetectors were measured by a Noise Measurement System (Platform-DA, NC300).

Supporting Information

Supporting Information is available from the Wiley Online Library or from the author.

Acknowledgements

D.Z. and H.F. contributed equally to this work. W.H., J.W., and L.L. conceived and supervised the research. D.Z. did the nanowire growth. D.Z. and H.F. fabricated the devices. D.Z., H.F., and P.W. performed the measurements. H.F. carried out the FDTD simulations. W.H., L.L., J.W., and D.Z. wrote the paper. All authors discussed the results and revised the manuscript. This work was partially supported by the Major State Basic Research Development Program (Grants 2014CB921600 and 2016YFA0203900), Natural Science Foundation of China (Grants 11322441, 61674157, 61574101, 61521005, and 61574152), Fund of Shanghai Science and Technology Foundation (Grants 13JC1408800 and 14JC1406400), CAS Interdisciplinary Innovation Team, and Ten Thousand Talents Program for Young Talents.

Received: June 23, 2016
Revised: August 11, 2016
Published online: September 14, 2016

[1] G. Konstantatos, E. H. Sargent, *Nat. Nanotechnol.* **2010**, *5*, 391.
[2] X. Liu, L. Gu, Q. Zhang, J. Wu, Y. Long, Z. Fan, *Nat. Commun.* **2014**, *5*, 4007.
[3] C. Soci, A. Zhang, B. Xiang, S. A. Dayeh, D. P. R. Aplin, J. Park, X. Y. Bao, Y. H. Lo, D. Wang, *Nano Lett.* **2007**, *7*, 1003.
[4] L. Hu, J. Yan, M. Liao, L. Wu, X. Fang, *Small* **2011**, *7*, 1012.
[5] X. S. Fang, Y. Bando, M. Y. Liao, U. K. Gautam, C. Y. Zhi, B. Dierre, B. D. Liu, T. Y. Zhai, T. Sekiguchi, Y. Koide, D. Golberg, *Adv. Mater.* **2009**, *21*, 2034.
[6] F. Gonzalez-Posada, R. Songmuang, M. Den Hertog, E. Monroy, *Nano Lett.* **2012**, *12*, 172.
[7] O. Lopez-Sanchez, D. Lembke, M. Kayci, A. Radenovic, A. Kis, *Nat. Nanotechnol.* **2013**, *8*, 497.
[8] X. Wang, P. Wang, J. Wang, W. Hu, X. Zhou, N. Guo, H. Huang, S. Sun, H. Shen, T. Lin, M. Tang, L. Liao, A. Jiang, J. Sun, X. Meng, X. Chen, W. Lu, J. Chu, *Adv. Mater.* **2015**, *27*, 6575.
[9] Y. T. Lee, P. J. Jeon, K. H. Lee, R. Ha, H. J. Choi, S. Im, *Adv. Mater.* **2012**, *24*, 3020.
[10] N. H. Van, J. H. Lee, J. I. Sohn, S. Cha, D. Whang, J. M. Kim, D. J. Kang, *Nanotechnology* **2014**, *25*, 205201.
[11] S. K. Hwang, S. Y. Min, I. Bae, S. M. Cho, K. L. Kim, T. W. Lee, C. Park, *Small* **2014**, *10*, 1976.
[12] D. Zheng, J. Wang, W. Hu, L. Liao, H. Fang, N. Guo, P. Wang, F. Gong, X. Wang, Z. Fan, X. Wu, X. Meng, X. Chen, W. Lu, *Nano Lett.* **2016**, *16*, 2548.
[13] M. Su, Z. Yang, L. Liao, X. Zou, J. C. Ho, J. Wang, J. Wang, W. Hu, X. Xiao, C. Jiang, C. Liu, T. Guo, *Adv. Sci.* **2016**, DOI: 10.1002/advs.201600078.
[14] X. F. Duan, Y. Huang, R. Agarwal, C. M. Lieber, *Nature* **2003**, *421*, 241.
[15] J. Cai, J. Jie, P. Jiang, D. Wu, C. Xie, C. Wu, Z. Wang, Y. Yu, L. Wang, X. Zhang, Q. Peng, Y. Jiang, *Phys. Chem. Chem. Phys.* **2011**, *13*, 14663.
[16] B. Piccione, C. H. Cho, L. K. van Vugt, R. Agarwal, *Nat. Nanotechnol.* **2012**, *7*, 640.
[17] L. Li, H. Lu, Z. Yang, L. Tong, Y. Bando, D. Golberg, *Adv. Mater.* **2013**, *25*, 1109.
[18] Y. Ye, Y. Dai, L. Dai, Z. Shi, N. Liu, F. Wang, L. Fu, R. Peng, X. Wen, Z. Chen, Z. Liu, G. Qin, *ACS Appl. Mater. Interfaces* **2010**, *2*, 3406.
[19] K. Heo, H. Lee, Y. Park, J. Park, H.-J. Lim, D. Yoon, C. Lee, M. Kim, H. Cheong, J. Park, J. Jian, S. Hong, *J. Mater. Chem.* **2012**, *22*, 2173.
[20] L. Zhu, C. Feng, F. Li, D. Zhang, C. Li, Y. Wang, Y. Lin, S. Ruan, Z. Chen, *RSC Adv.* **2014**, *4*, 61691.
[21] L. Li, Z. Lou, G. Shen, *ACS Appl. Mater. Interfaces* **2015**, *7*, 23507.
[22] X. Liu, L. Jiang, X. Zou, X. Xiao, S. Guo, C. Jiang, X. Liu, Z. Fan, W. Hu, X. Chen, W. Lu, W. Hu, L. Liao, *Adv. Mater.* **2014**, *26*, 2919.
[23] C. Zhang, Z. Xu, W. Tian, D. M. Tang, X. Wang, Y. Bando, N. Fukata, D. Golberg, *Nanotechnology* **2015**, *26*, 154001.
[24] T.-Y. Wei, C.-T. Huang, B. J. Hansen, Y.-F. Lin, L.-J. Chen, S.-Y. Lu, Z. L. Wang, *Appl. Phys. Lett.* **2010**, *96*, 013508.
[25] D. Wu, Y. Jiang, Y. Zhang, Y. Yu, Z. Zhu, X. Lan, F. Li, C. Wu, L. Wang, L. Luo, *J. Mater. Chem.* **2012**, *22*, 23272.
[26] P. Guo, W. Hu, Q. Zhang, X. Zhuang, X. Zhu, H. Zhou, Z. Shan, J. Xu, A. Pan, *Adv. Mater.* **2014**, *26*, 2844.
[27] L. Li, P. Wu, X. Fang, T. Zhai, L. Dai, M. Liao, Y. Koide, H. Wang, Y. Bando, D. Golberg, *Adv. Mater.* **2010**, *22*, 3161.
[28] X. Xing, Q. Zhang, Z. Huang, Z. Lu, J. Zhang, H. Li, H. Zeng, T. Zhai, *Small* **2016**, *12*, 874.
[29] P. Wang, P. Deng, Y. Nie, Y. Zhao, Y. Zhang, L. Xing, X. Xue, *Nanotechnology* **2014**, *25*, 075501.
[30] R. M. Ma, L. Dai, H. B. Huo, W. J. Xu, G. G. Oin, *Nano Lett.* **2007**, *7*, 3300.
[31] E. J. Lee, K. Balasubramanian, R. T. Weitz, M. Burghard, K. Kern, *Nat. Nanotechnol.* **2008**, *3*, 486.
[32] J. Miao, W. Hu, N. Guo, Z. Lu, X. Liu, L. Liao, P. Chen, T. Jiang, S. Wu, J. C. Ho, L. Wang, X. Chen, W. Lu, *Small* **2015**, *11*, 936.
[33] M. Freitag, J. C. Tsang, A. Bol, D. N. Yuan, J. Liu, P. Avouris, *Nano Lett.* **2007**, *7*, 2037.
[34] T. Dufaux, M. Burghard, K. Kern, *Nano Lett.* **2012**, *12*, 2705.
[35] W. Qiu, W. Hu, *Sci. China-Phys. Mech. Astron.* **2015**, *58*, 027001.

© 2016 WILEY-VCH Verlag GmbH & Co. KGaA, Weinheim

[36] W. Choi, M. Y. Cho, A. Konar, J. H. Lee, G. B. Cha, S. C. Hong, S. Kim, J. Kim, D. Jena, J. Joo, S. Kim, *Adv. Mater.* **2012**, *24*, 5832.
[37] H. Kind, H. Q. Yan, B. Messer, M. Law, P. D. Yang, *Adv. Mater.* **2002**, *14*, 158.
[38] N. Guo, W. Hu, L. Liao, S. Yip, J. C. Ho, J. Miao, Z. Zhang, J. Zou, T. Jiang, S. Wu, X. Chen, W. Lu, *Adv. Mater.* **2014**, *26*, 8203.
[39] J. S. Jie, W. J. Zhang, Y. Jiang, X. M. Meng, Y. Q. Li, S. T. Lee, *Nano Lett.* **2006**, *6*, 1887.
[40] X. Gong, M. H. Tong, Y. J. Xia, W. Z. Cai, J. S. Moon, Y. Cao, G. Yu, C. L. Shieh, B. Nilsson, A. J. Heeger, *Science* **2009**, *325*, 1665.
[41] J. S. Miao, W. D. Hu, N. Guo, Z. Y. Lu, X. M. Zou, L. Liao, S. X. Shi, P. P. Chen, Z. Y. Fan, J. C. Ho, T. X. Li, X. S. Chen, W. Lu, *ACS Nano* **2014**, *8*, 3628.
[42] J. R. Manders, T. H. Lai, Y. B. An, W. K. Xu, J. Lee, D. Y. Kim, G. Bosman, F. So, *Adv. Funct. Mater.* **2014**, *24*, 7205.
[43] S. P. Chang, C. Y. Lu, S. J. Chang, Y. Z. Chiou, T. J. Hsueh, C. L. Hsu, *IEEE J. Sel. Top. Quantum Electron.* **2011**, *17*, 990.
[44] C. T. Lee, T. S. Lin, H. Y. Lee, *IEEE Photonics Technol. Lett.* **2010**, *22*, 1117.
[45] H. Y. Liu, S. H. Hong, W. C. Sun, S. Y. Wei, S. M. Yu, *IEEE Trans. Electron Devices* **2016**, *63*, 79.

© 2016 WILEY-VCH Verlag GmbH & Co. KGaA, Weinheim